CELL CYCLE
2021, VOL. 20, NO. 4, 417–433
https://doi.org/10.1080/15384101.2021.1877936

Taylor & Francis
Taylor & Francis Group

RESEARCH PAPER

Nitric oxide attenuates microglia proliferation by sequentially facilitating calcium influx through TRPV2 channels, activating NFATC2, and increasing p21 transcription

Matthew J.E. Maksoud[a,b], Vasiliki Tellios[a,b], and Wei-Yang Lu[a,b,c]

[a]Graduate Program of Neuroscience, The University of Western Ontario, London, Canada; [b]Translational Neuroscience Research Group, Robarts Research Institute, The University of Western Ontario, London, Canada; [c]Department of Physiology and Pharmacology, University of Western Ontario, London, Canada

ABSTRACT

Microglia proliferation is critical for proper development and function of the central nervous system (CNS), while dysregulation of proliferation contributes to pathology. We recently reported that male inducible nitric oxide synthase knockout (iNOS$^{-/-}$) mice displayed significantly more proliferating microglia in their postnatal cortex than age-matched wildtype (WT) male mice. Moreover, nitric oxide (NO) signaling in mouse microglia greatly upregulates calcium entry through transient receptor potential vanilloid type 2 (TRPV2) channels. Considering that TRPV2 activity restricts astrocytic proliferation within glioma tissues, we investigated the roles of iNOS/NO signaling and TRPV2 expression in the regulation of microglial proliferation in vitro using assays of calcium imaging, immunocytochemistry, western blot, and polymerase chain reaction. Results showed that non-dividing microglia exhibited substantially higher expression of TRPV2 on the plasma membrane and significantly larger calcium influx through TRPV2 channels in comparison to dividing microglia. Additionally, non-dividing WT microglia exhibited significantly more NO production than dividing WT microglia. Furthermore, the NO-donor NOC18 increased the nuclear translocation of nuclear factor of activated T-cells cytoplasmic 2 (NFATC2) and the mRNA of the cyclin-dependent kinase inhibitor p21 and decreased the percentage of dividing WT and iNOS$^{-/-}$ microglia in culture. Importantly, the presence of the TRPV2 inhibitor tranilast abolished these effects of NOC18. Together, results from this study indicated that iNOS/NO signaling inhibits microglial proliferation through TRPV2-mediated calcium influx, nuclear translocation of the transcription factor NFATC2, and p21 expression.

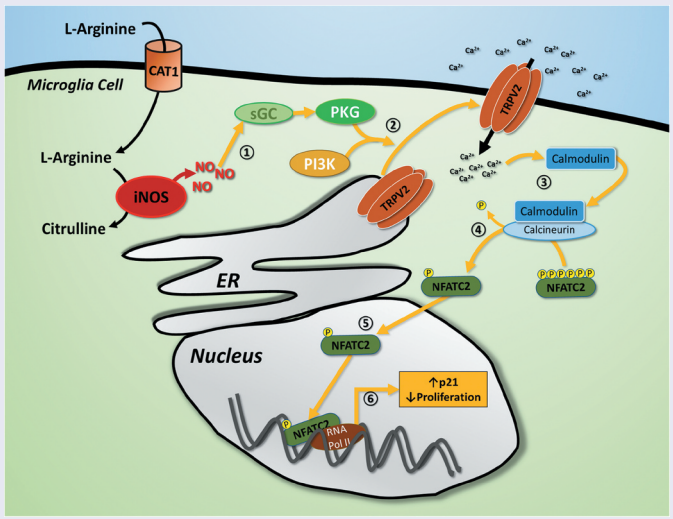

Proposed molecular mechanism by which NO-TRPV2 signaling regulates microglia proliferation *in vitro*.

ARTICLE HISTORY
Received 31 August 2020
Revised 13 January 2021
Accepted 14 January 2021

KEYWORDS
Calcium; nitric oxide; cell cycle; NFAT; p21; TRPV2

CONTACT Wei-Yang Lu Email wlu53@uwo.ca
Supplemental data for this article can be accessed here.

Introduction

Microglia are essential immune cells of the central nervous system (CNS) that produce copious amounts of nitric oxide (NO) via inducible nitric oxide synthase (iNOS) to regulate their own cellular functions such as proliferation [1–4]. Aberrant microglia proliferation and iNOS expression contribute to neurological disease progression. It has been shown that microglia are the most prominent immune cells that infiltrate and proliferate within gliomas [5], while also exhibiting reduced iNOS expression [6,7] and secreting anti-inflammatory cytokines such as IL-10 and TGFβ1 [8–10]. A positive correlation between glioma malignancy and the number of alternatively activated microglia present within the glioma suggests that microglia contribute to glioma pathology [11–13].

Previous studies also implicated iNOS expression in Alzheimer's like pathology progression [14–16]. For example, using a double transgenic mouse model for Alzheimer's disease that expressed Swedish mutation of the amyloid precursor protein together with presenilin-1 deletion in exon 9 demonstrated cognitive deficits, decreased iNOS mRNA expression, as well as increased microglia proliferation at 6 months of age when compared to age-matched WT mice [14]. Evidently, iNOS-NO signaling critically regulates microglia proliferation; however, the underlying molecular mechanism that regulates microglia proliferation remains unclear [17]. We recently demonstrated that mice lacking iNOS expression ($iNOS^{-/-}$) displayed significantly more proliferating microglia in the cortex during early postnatal development than that of age-matched WT mice [18]. Moreover, we demonstrated that iNOS-NO signaling impedes cell-cycle progression of microglia through cyclic guanosine-monophosphate (cGMP) activation of protein kinase G (PKG) signaling [18]. These novel findings indicate that the iNOS-NO-cGMP-PKG signaling cascade critically restricts microglia proliferation.

The transient receptor potential vanilloid type 2 (TRPV2) ion channel is highly calcium permeable and largely implicated in cellular proliferation, differentiation, and cancer progression [19], while also highly expressed in microglia and other glia cells [20–22]. Previous studies demonstrated that TRPV2 expression attenuates astrocytic glioblastoma cell proliferation [20,21] and clearly established a crucial role of TRPV2 channel activity in restricting cell proliferation. Interestingly, we have recently shown that activation of iNOS-NO-cGMP-PKG cascade traffics TRPV2 channel proteins from the endoplasmic reticulum to the plasma membrane to intensify calcium influx in murine microglia [2].

This present study set out to examine if NO-mediated TRPV2-trafficking and subsequent calcium entry attenuates microglia proliferation. Using multiple imaging techniques on primary WT and $iNOS^{-/-}$ murine microglia cultures we examined the TRPV2 surface expression and calcium influx in different cell-cycle stages while exploring subsequent gene expression. Our results showed that NO-TRPV2 signaling critically regulates microglia proliferation whereby actively dividing microglia exhibited less TRPV2 plasma membrane expression and calcium influx, less nuclear expression of nuclear factor of activated T-cells cytoplasmic-2 (NFATC2), and decreased p21 mRNA expression, compared to nondividing microglia. Future studies examining NO-TRPV2-NFATC2-p21 signaling in microglia may uncover the impact that microglia proliferation contributes to the progression of pathologies in the CNS.

Materials and methods

Materials, compounds, and treatments

Materials and compounds were purchased from the following sources – phosphate-buffered saline (PBS), paraformaldehyde (PFA), 4',6-diamidino-2-phenylindole (DAPI), triton, glycine, poly-D-lysine (PDL), sucrose, glycerol, ethylene glycol, 4-(2-hydroxyethyl)-1-piperazineethanesulfonic acid (HEPES) (Millipore-Sigma, Oakville, ON); Dulbecco's modified eagle medium (DMEM), fetal bovine serum (FBS), trypsin, sodium-pyruvate, penicillin/streptomyocin (P/S), Leibowitz L-15 media, bovine serum albumen (BSA) (ThermoFischer Scientific, Waltham, MA); normal donkey serum (NDS) (Jackson Immunoresearch Laboratories, inc., West Grove, PA); Fluormount-G (Electron Microscopy Solutions, Hatfield, PA), calcium fluorescent dye: Rhod-4AM, NO-sensitive fluorescent dye: DAX-J2 (AAT Bioquest, Sunnyvale, CA).

Treatment concentrations were adapted from previous literature and purchased from the following sources – slow-release NO-donor: diethylenetriamine NONOate (NOC18, 100 μM), NOS inhibitor: G-nitro-L-arginin-methyl ester (L-NAME, 100 μM), arginyl-lysyl-arginyl-alanyl-arginyl-lysyl-glutamic acid (PKG inhibitory peptide; PKG_i, 10 μM), 8-bromo-cyclic guanosine monophosphate (8Br-cGMP, 10 μM) (Cayman Chemical, Ann Arbor, MI); TRPV2 agonist: 2-aminoethoxydiphenyl borate (2APB, 250 μM) (Santa Cruz Biotechnology, Dallas, TX); TRPV2 agonist: probenecid (100 μM), TRPV2 inhibitor: tranilast (75 μM) (Tocris Bioscience, Oakville, ON); iNOS substrate: L-arginine (100 μM) (Millipore-Sigma, Oakville, ON).

Primary microglia cultures

WT (C57BL/6, Stock No: 000664) and $iNOS^{-/-}$ ($B6.129P2\text{-}Nos2^{tm1Lau}$, Stock No: 002609) mice

purchased from The Jackson Laboratory. All experiments were conducted in accordance with the Animal Care and Veterinary Services at The University of Western Ontario, Canada. Microglia were isolated and cultured as previously described to yield cultures of 95% pure primary microglia [18]. WT microglia cultures were used to examine the influence of endogenous iNOS/NO signaling on microglia cell-cycle progression while $iNOS^{-/-}$ microglia cultures were utilized to examine how the absence of endogenous iNOS/NO signaling influences microglia cell-cycle progression. Briefly, cortices isolated from male and female postnatal day 0–4 WT or $iNOS^{-/-}$ mice and placed in ice-cold Leibowitz L-15 media. Next, cortices were homogenized, filtered through a 70 μm nylon filter, and centrifuged for 4 minutes at 900 g. The cell pellet was resuspended in DMEM containing 1 × P/S and 10% FBS. The collected cortical cells were cultured in T-75 flasks for 2 weeks, with media changes occurring every 3 days. After 2 weeks, T-75 flasks were shaken for 2hrs at 36°C and 200rpm. The media containing detached microglia was centrifuged at 900 g for 4 min, and the supernatant was removed. The microglia cell pellet was resuspended in fresh culture media and plated at 5×10^4 cells/ml for experiments. Microglia were allowed to rest overnight in DMEM supplemented with 2.5% FBS, 5% sodium-pyruvate, and 1% P/S, under culture conditions of 37°C and 5% CO_2 before conducting experiments.

BV2 cell-line cultures

BV2 microglia were generously gifted to us from Dr. Michael J. Strong at The University of Western Ontario. BV2 microglia were utilized for immunoblot analyses to avoid euthanizing a large number of postnatal day 0–4 mice to obtain enough protein from primary microglia cultures. BV2 cells were cultured in DMEM containing 1 × P/S and 10% FBS at normal conditions of 5% CO_2 at 37°C. Once BV2 cell confluency reached 70%, cells were washed with PBS and incubated for 2 min in 0.25% trypsin in PBS to facilitate detachment. Trypsin was neutralized using equal parts of culture media containing FBS, and BV2 cells were passaged 1:40 into a new culture vessel with DMEM containing 1 × P/S and 10% FBS 3 × a week. For experiments, BV2 cells were plated at 5×10^4 cells/ml in DMEM supplemented with 2.5% FBS, 5% sodium-pyruvate, and 1% P/S, and allowed to rest overnight before conducting experiments.

Immunocytochemistry

Primary microglia and BV2 cells cultured on glass coverslips underwent experimental treatments at previously mentioned concentrations, for 48 hrs under normal culture conditions of 37°C and 5% CO_2. After 48 hrs, culture media was removed and cells were fixed using 4% PFA for 5 min. Fixed microglia were washed with 0.1 M glycine in PBS, followed by two PBS washes of 5 min each. Cell membrane permeabilization occurred using 0.1% triton in PBS for 5 min, followed by a 1 h incubation with blocking solution containing 5% NDS in PBS to decrease nonspecific antibody binding.

To determine the cell-cycle stages of microglia, primary CD11b (rat, BioRAD #MCA275R, 1:150) and Ki67 (rabbit, AbCam #ab15580, 1:300) antibodies in 1% NDS in PBS were incubated on coverslips for 2 hrs. The secondary antibodies – Cy3 and Alexa Fluor-647 (Jackson Immunoresearch, West Grove, PA) – were incubated in 1% NDS in PBS for 1 h. Following three washes in PBS, microglia were incubated with the primary antibody phosphorylated histone 3 (S10+ T11) conjugated to Alexa Fluor 488 (rabbit, AbCam #ab200614, 1:5000) in 1% NDS in PBS for 2hrs.

To examine subcellular localization of TRPV2, microglia were incubated with TRPV2 (Guinea pig, Alomone Labs #AGP-033, 1:100) and Ki67 (rabbit, AbCam #ab15580, 1:300) antibodies in 1% NDS in PBS were incubated on coverslips for 2 hrs. The secondary antibodies – Cy3 and Alexa Fluor-647 (Jackson Immunoresearch, West Grove, PA) – were incubated in 1% NDS in PBS for 1 h. Following three washes in PBS, microglia were incubated with the primary antibody phosphorylated histone 3 (S10+ T11) conjugated to Alexa Fluor 488 (rabbit, AbCam, #ab200614, 1:5000) in 1% NDS in PBS for 2hrs. Analysis for localizing TRPV2 fluorescence within microglia was adapted from [2].

To examine subcellular localization of NFATC2, microglia were incubated with primary antibodies for CD11b (rat, BioRAD #MCA275R, 1:150) and NFATC2 (mouse, Thermo Fisher Scientific #MA1-025, 1:200) in 1% NDS in PBS for 2hrs. Next, microglia were incubated with the secondary antibodies Cy3 and Alexa-Fluor-488 in 1% NDS in PBS for 1 h. Secondary

antibodies were removed and microglia were washed 3× with PBS for 10 min each before DAPI staining (1 µg/ml) for 10 min. Microglia were mounted onto slides using Fluormount-G. Images were taken using the Olympus FV-1000 confocal laser scanning microscope through a 60× oil immersion objective.

Calcium imaging and cell-cycle classification

For calcium-imaging, microglial cultures were grown in 24-well plates and DMEM culture media was washed out with bath solution containing (in mM): 130 NaCl, 5 KCl, 3 $MgCl_2$, 2 $CaCl_2$, 5 glucose, and 10 HEPES. Rhod-4AM was equilibrated to room temperature for 1 hr before incubating microglia cultures with 3 µM rhod-4AM under normal conditions for 1 hr. Rhod-4AM was washed out of cells using bath solution. The intracellular fluorescent intensity of rhod-4 within microglia were imaged in 10 second intervals using the EVOS FL Auto system under 20× magnification. Baseline levels of rhod-4 fluorescence were recorded before 2APB (250 µM) application. Intracellular rhod-4 fluorescent changes in each cell were normalized to the average baseline level within the imaging field using FIJI open-source software [23].

As previously described [18], microglial cell-cycle stages were classified based on the immuno-detection of cell-cycle markers. After calcium imaging, microglia were subjected to immunocytochemistry of cell-cycle markers. Microglial cells were identified by the expression of CD11b, and only CD11b positive cells were included in the image analyses. Using FIJI open-source software [23], microglia were classified into three different cell-cycle phases: G0 microglia display nuclear DAPI fluorescence; interphase microglia exhibited nuclear fluorescence of DAPI and Ki67; or microglia in mitosis displayed nuclear fluorescence of DAPI and pH3. As outlined in **Supplemental Figure 1**, the calcium response in each microglia was grouped and then averaged based on the cell-cycle phase it presented in. The normalized rhod-4 fluorescence intensity for microglia in each cell-cycle stage were plotted versus time of imaging using Excel.

NO-imaging and cell-cycle classification

Intracellular DAX-J2 fluorescence was used to measure free NO production in microglial cultures. WT or BV2 microglia were cultured in 24-well plates and culture media was washed out with the same bath solution used in calcium imaging. DAX-J2 was equilibrated to room temperature for 1 hr before incubating microglia cultures in 4 µM DAX-J2 for 45 min under normal conditions. After washing out extracellular DAX-J2, NO-imaging was performed using the EVOS-FL Auto system under 20× magnification for 20 min. Baseline fluorescent levels of DAX-J2 were recorded before application of the iNOS substrate L-arginine (100 µM), and intracellular DAX-J2 fluorescent changes in each cell within the imaging field were normalized to the average baseline level using FIJI open-source software [23].

After NO-imaging, cells were washed 3× with PBS and immunocytochemistry was carried out to probe for the cell-cycle markers pH3, Ki67, and DAPI as previously described. The microglia within the DAX-J2-imaging field were relocated and grouped based on their expressed cell-cycle markers. Any microglia that were washed away during the immunostaining process were removed from the analysis. The averaged normalized intensity of DAX-J2 fluorescence for each microglia was plotted versus time according to the cell-cycle phases using Excel.

NFATC2 localization analysis

Localization analysis for NFATC2 expression within microglia is outlined in **Supplemental Figure 2**. Briefly, microglia stained with CD11b, NFATC2, and DAPI were imaged using the Olympus FV-1000 microscope. The DAPI and CD11b fluorescent channels were individually thresholded using constant settings. The particle analyzer function within FIJI [23] was used to determine the region of interest (ROI) for the nuclear and entire cell regions for individual microglia using the DAPI and CD11b fluorescent channels, respectively. The nuclear ROIs were subtracted from the entire cell ROIs to produce the cytosolic ROIs for each microglia. The nuclear and cytosolic ROIs were overlaid onto the NFATC2 channel for quantifying fluorescent intensity of NFATC2 within the nucleus and cytoplasm of each microglia. A ratio of nuclear/cytoplasmic NFATC2 fluorescence for each microglia was determined to control for variability in fluorescent intensity and cell size between images and individual microglia. Normalized nuclear/cytoplasmic NFATC2 fluorescent intensity was graphed using Excel.

Western blot

To quantify the NFATC2 expression in microglia, the BV2 cell line was used for western blot assays. Cultured BV2 microglia were washed 3× with PBS before being scraped into Eppendorf tubes and lysed using 150 µL of radioimmunoprecipitation assay buffer. BV2 lysates were centrifuged at 13,000 g for 5 min, and the supernatant containing proteins was quantified using Bradford assay (Bio-Rad, Hercules, CA). Proteins from different treatment groups were run through SDS-PAGE using an 8% polyacrylamide gel at 100 V before being transferred to a polyvinylidene difluoride membrane. Membranes were blocked for 1 hr using 5% BSA before being incubated with NFATC2 (ThermoFisher Scientific, Waltham, MA) antibody at 1:1000 dilution. Secondary anti-mouse IgG horseradish peroxidase (HRP) conjugate (1:5000) (Jackson Immunoresearch, Burlington, ON) was then incubated with the membrane for 1.5hrs. NFATC2 protein was normalized to the housekeeping protein glyceraldehyde 3-phosphate dehydrogenase (GAPDH) (1:10,000) (Abcam Inc., Cambridge, MA). Protein bands were visualized using enhanced chemiluminescent substrate (Bio-Rad, Hercules, CA) and imaged using the Biod-Rad VersaDoc imaging system. Experimental N-values represent the number of individual wells in which cell-lysates were collected from each treatment group.

Reverse transcription-quantitative polymerase chain reaction (RT-qPCR)

Total RNA was isolated using RNeasy Mini Kit (Qiagen, Toronto, ON) from primary WT or iNOS$^{-/-}$ microglia cultured on 60 mm dishes as per manufacturer's instructions. Reverse transcription using qScript^{TM} XLT cDNA SuperMix (Quantabio, Beverly, MA) was carried out on 1 µg of extracted microglial RNA. Quantitative PCR was conducted using PerfeCTa® SYBR® Green FastMix® for iQ (Quantabio, Beverly, MA), 25ng of cDNA template, and 500 nM of forward and reverse primers specific to the gene of interest, as per manufacturer's instructions. Forward and reverse primers for murine p21 were as follows: forward 5′CATCTCAGGGCCGAAAACGG3′, reverse 5′CAGGCCTCTTGCAGGATCTTT3′. The qPCR reactions were run in triplicate 25 µL reactions with a no template control on a BioRad MyiQ Single-color Real-Time PCR detection system (Biorad, Mississauga, ON), with a 40-cycle protocol. The differences in cycle thresholds between the genes of interest and the reference gene β-actin forward 5′CTGTCCCTGTATGCCTCTG3′, reverse 5′ATGTCACGCACGATTTCC3′, were normalized to the control treatment levels using the ΔCt method and graphed using excel.

Statistics. Statistical analyses were done using Graphpad Prisim 8. All results are shown as mean ± SEM. A one-way ANOVA with Tukey's post hoc comparison was used when comparing three or more groups with P-values of less than 0.05 taken as showing significant differences between means.

Results

Nondividing WT and BV2 microglia display increased NO production in the presence of L-arginine

To correlate the enzymatic activity of iNOS to the cell-cycle stages of microglia, we performed DAX-J2 fluorescent imaging to assess the levels of NO production within individual WT and BV2 microglia in response to the NOS substrate L-arginine (100 µM), followed by immunocytochemistry to probe for the cell-cycle markers Ki67 and pH3. Results demonstrated that after application of L-arginine, microglia in the G0 cell-cycle stage displayed gradual and sustained production of NO; while dividing microglia in interphase or mitosis, which were Ki67- and/or pH3-positive, displayed a decline in NO production (Figures 1a and Figures 1b). Together, this data suggests that a higher level of NO production occurs in non-dividing microglia.

Plasma membrane expression of TRPV2 is decreased in dividing microglia

Considering that NO production is decreased in actively dividing microglia, and that NO is critical

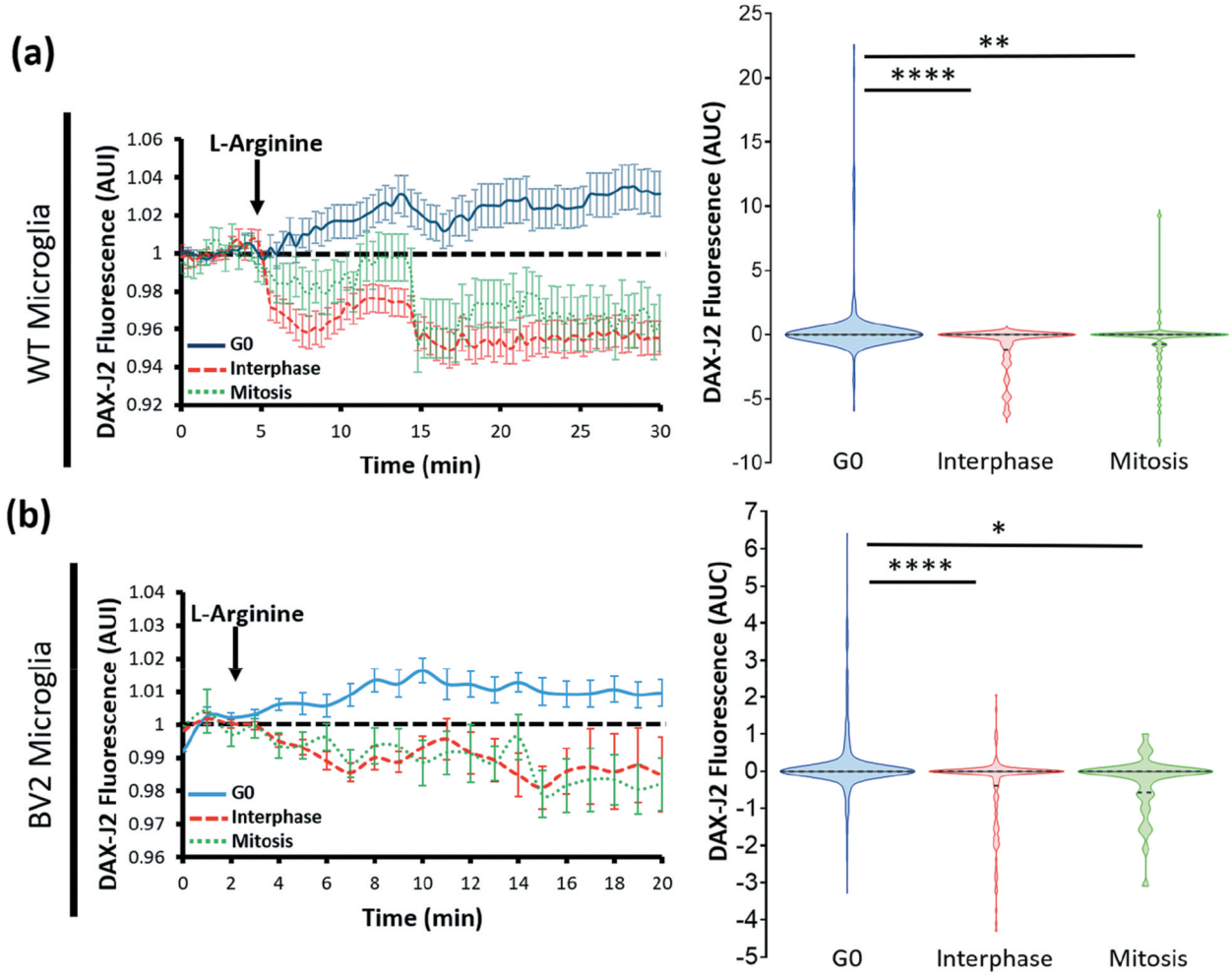

Figure 1. Nondividing WT and BV2 microglia display increased NO production in the presence of L-arginine. *Left panels*: Changes in DAX-J2 fluorescent intensity with time in response to L-arginine (100 μM) treatment in (a) WT and (b) BV2 microglia present in G0 (blue), interphase (red), and mitotic (green) cell-cycle stages. *Right panels*: Violin plots depict the area under the NO-dynamic curve (AUC) as a distribution of all cells. Solid black lines mark the median values while dotted lines indicate the interquartile ranges for **(a)** WT and **(b)** BV2 microglia in G0, interphase, and mitosis respectively. Statistical comparisons were determined from n = 190 G0 WT cells; n = 93 interphase WT cells; n = 63 mitotic WT cells; and n = 353 G0 BV2 cells; n = 193 interphase BV2 cells; n = 42 mitotic BV2 cells from multiple imaged fields from N= 4 and N= 5 wells respectively, and $p < 0.05$ using a one-way ANOVA and Tukey's post-hoc comparison between cell-cycle stages. *$p < 0.05$, **$p < 0.01$, ****$p < 0.0001$.

for the plasma membrane expression of TRPV2 [2], we examined whether the subcellular localization of TRPV2 changes in murine microglia cell-cycle stages.

To this end, we conducted immunocytochemistry to probe for TRPV2, Ki67, pH3, and DAPI in WT, iNOS$^{-/-}$, and BV2 microglia. Our confocal microscopy analyses displayed significantly more localization of TRPV2 proteins on the plasma membrane versus the cytosol within nondividing microglia when compared to dividing microglia in interphase or mitosis (Figure 2a-c; one-way ANOVA; WT microglia, F (2,44) = 10.48; n = 16 G0, n = 15 interphase, n = 16 mitotic microglia; p = 0.0002; iNOS$^{-/-}$ microglia, F (2,56) = 8.431; n = 16 G0, n = 19 interphase, n = 24 mitotic microglia; p = 0.0006; BV2, F (2,31) = 35.51; n = 9 G0, n = 11 interphase, n = 14 mitotic microglia; $p < 0.0001$). There was no significant difference in the ratio of plasma membrane versus internal membrane localization of TRPV2 between interphase and mitotic murine microglia, which all displayed a high internal localization of TRPV2. Importantly, nondividing iNOS$^{-/-}$ microglia displayed significantly less plasma membrane versus internal membrane localization of TRPV2 when compared to nondividing WT and/or BV2 microglia (data not shown; one-way ANOVA; F (2,38) = 4.581; n = 16 G0 WT, n = 15 G0 iNOS$^{-/-}$, n = 9 G0 BV2; p = 0.0165). Together, this data demonstrates that the plasma membrane localization of TRPV2 is highest in nondividing microglia and decreases in dividing microglia, in accordance with the change in NO production at the different cell-cycle stages.

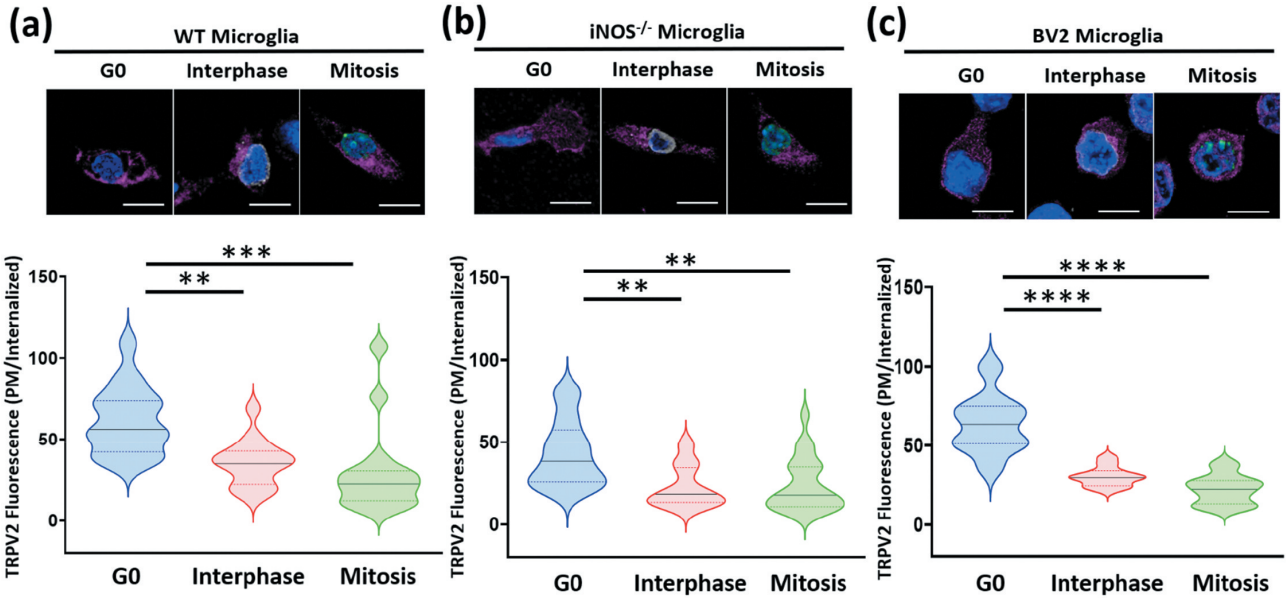

Figure 2. Plasma membrane expression of TRPV2 is decreased in dividing microglia. *Top panels*: Representative images of TRPV2 (purple), Ki67 (gray), pH3 (green), and DAPI (blue) immunostaining, in (a) WT, (b) iNOS$^{-/-}$, and (c) BV2 microglia. Scale bars represent 10 µm. *Bottom panels*: Violin plots depict plasma membrane/internalized TRPV2 fluorescent intensity (mean arbitrary units ± SEM) in **(a)** WT, **(b)** iNOS$^{-/-}$, and **(c)** BV2 microglia in G0, interphase, or mitosis. Solid black lines mark the median values while dotted lines indicate the interquartile ranges. Significance was determined from n = 16 G0, n = 15 interphase, and n = 16 mitotic WT microglia; n = 16 G0, n = 19 interphase, and n = 24 mitotic iNOS$^{-/-}$ microglia; and n = 9 G0, n = 11 interphase, and n = 14 mitotic BV2 microglia, from at least N= 3 wells and a one-way ANOVA with Tukey's post-hoc comparison. $^{**}p < 0.01$, $^{***}p < 0.001$, $^{****}p < 0.0001$.

Activation of TRPV2 channels induces differential levels of calcium influx in microglia at different cell-cycle stages

We previously demonstrated that the TRPV1-3 agonist 2APB [24] evokes calcium entry into primary mouse microglia mainly by activation of TRPV2 channels and not TRPV1 or TRPV3 [2]. To examine the activity level of TRPV2 channels in different microglial cell-cycle stages, we assayed the 2APB (250 µM) induced intracellular calcium levels in WT, iNOS$^{-/-}$, and BV2 microglia, and then carried out immunocytochemistry to probe for the cell-cycle markers Ki67 and pH3. Results from these assays revealed that nondividing murine microglia displayed a significantly larger calcium influx upon 2APB administration in comparison to dividing microglia in interphase and/or mitosis (Figure 3a-c; one-way ANOVA; WT microglia, F (2,737) = 20.61; n = 558 G0, n = 140 interphase, n = 42 mitotic microglia; $p < 0.0001$; iNOS$^{-/-}$ microglia, F (2,276) = 45.76; n = 196 G0, n = 66 interphase, n = 18 mitotic microglia; $p < 0.0001$; BV2 microglia, F (2,609) = 34.33; n = 423 G0, n = 143 interphase, n = 46 mitotic microglia, $p < 0.0001$. In addition, nondividing WT and BV2 microglia displayed a larger area under the calcium dynamic curve in comparison to nondividing iNOS$^{-/-}$ microglia. Together, all available data suggests that nondividing microglia present with increased calcium influx through TRPV2 channels when compared to dividing microglia, which is due to a higher level of endogenous iNOS/NO signaling that upregulates the plasma membrane expression of TRPV2 proteins [2].

Pharmacological modulation of TRPV2 channel activity influences cell-cycle progression in primary microglia

Next, we examined if the NO-TRPV2 signaling pathway influences cell-cycle progression of primary microglia. Specifically, we examined the proportion of WT and iNOS$^{-/-}$ microglia that express the cell-cycle markers Ki67 and/or pH3 in the absence (control) and presence of either the slow-release NO-donor NOC18, the TRPV2 agonist

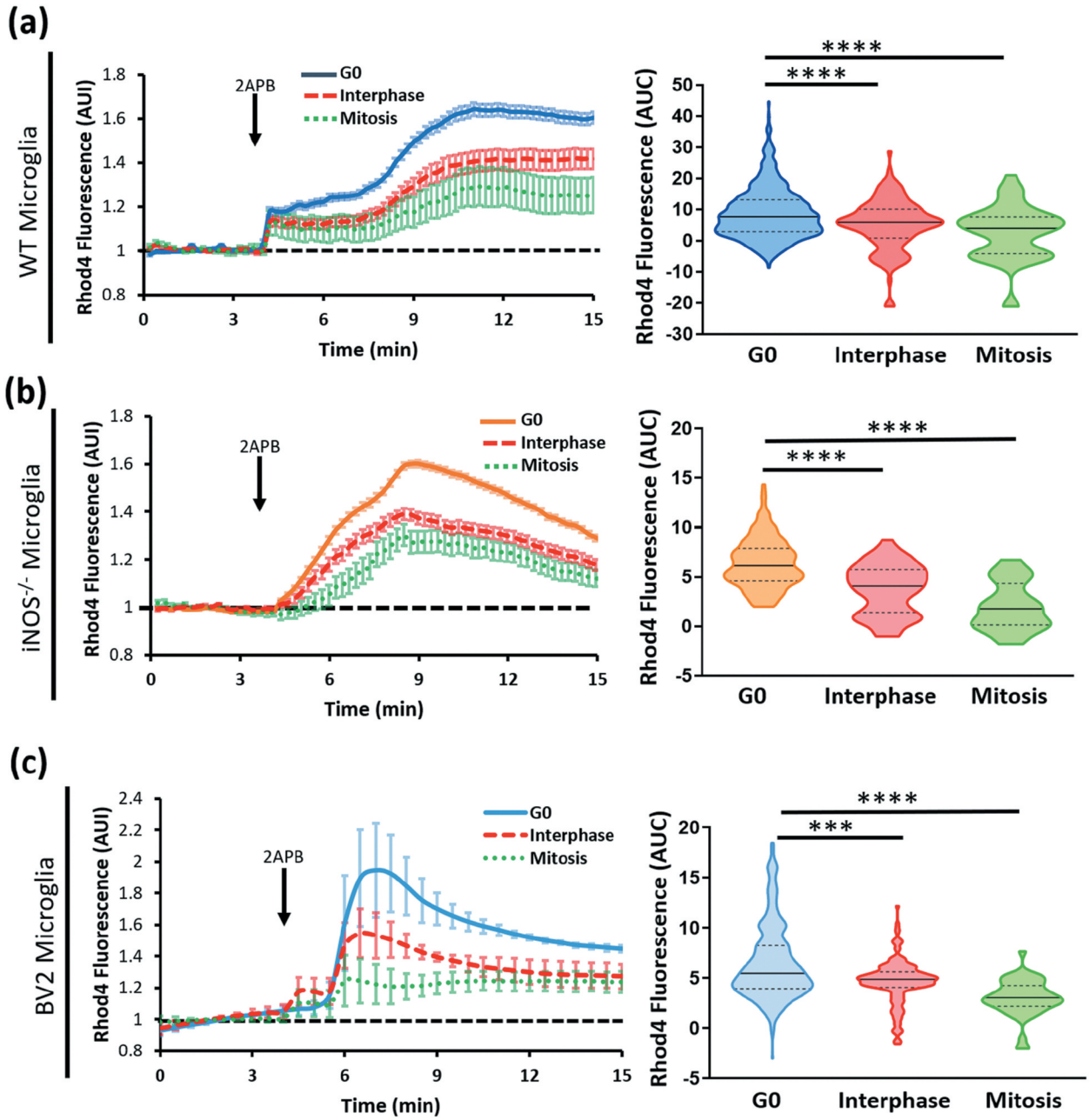

Figure 3. Activation of TRPV2 channels induces differential levels of calcium influx in microglia at different cell-cycle stages. *Left Panels*: Changes in rhod-4 fluorescent intensity with time in response to 2APB (250 µM) treatment on (a) WT, (b) iNOS$^{-/-}$, and (c) BV2 murine microglia in G0, interphase (red trace) and mitosis (green trace). *Right Panels*: Violin plots depict the area under the calcium dynamic curve (AUC) in response to 2APB treatment as a distribution of all **(a)** WT, **(b)** iNOS$^{-/-}$, and **(c)** BV2 microglia in G0, interphase (red), and mitosis (green). Solid black lines mark the median while dotted lines indicate the interquartile ranges for microglia. Statistical significance was determined from n = 558 G0; n = 140 interphase; n = 42 mitotic WT cells; n = 196 G0; n = 66 interphase; n = 18 mitotic iNOS$^{-/-}$ cells; and n = 423 G0; n = 143 interphase; n = 46 mitotic BV2 cells from N= 4 wells and $p < 0.05$ using a one-way ANOVA and Tukey's post-hoc comparison. ***$p < 0.001$, ****$p < 0.0001$.

probenecid, the TRPV2 antagonist tranilast, or a combination of NOC18 + tranilast.

Our assays revealed that WT microglia treated with NOC18 or probenecid resulted in a significantly larger percentage of nondividing cells that stained for DAPI only (Figures 4a and Figures 4b; one-way ANOVA; F (4,53) = 49.44; n = 14 control, n = 10 NOC18, n = 12 probenecid, n = 11 tranilast, n = 11 NOC18 + tranilast; $p < 0.0001$), and a significantly smaller percentage of dividing cells that expressed Ki67 and/or pH3 when compared to control microglia (Figures 4c and Figures 4d; one-way ANOVA; Interphase, F (4,53) = 32.28; n = 14 control, n = 10 NOC18, n = 12 probenecid, n = 11 tranilast, n = 11

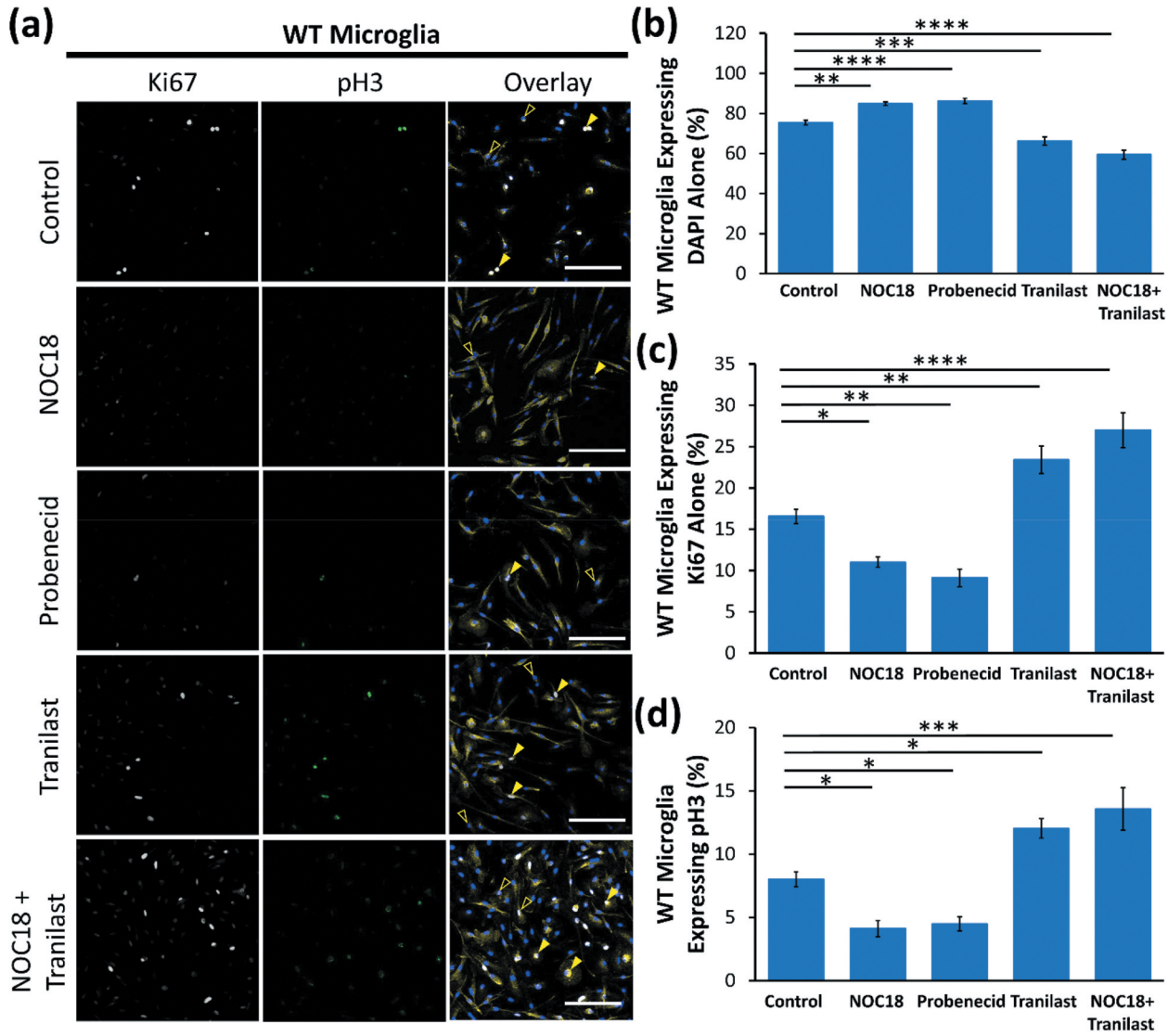

Figure 4. Pharmacological activation of TRPV2 channels restrict cell-cycle progression in primary WT microglia. (a) Representative images of Ki67 (gray), pH3 (green), CD11b (yellow), and DAPI fluorescence in WT microglia under control conditions or treated with NOC18 (100 µM), the TRPV2 agonist probenecid (100 µM) or the TRPV2 antagonist tranilast (75 µM), or a combination of NOC18 + tranilast for 48hrs. Scale bars represent 100 µm. Open arrows point to $Ki67^{+}$ microglia while closed arrows point to $pH3^{+}$ microglia. Bar graphs report the percentages ± SEM of WT microglia having nuclei stained with (b) DAPI alone, (c) DAPI and Ki67, or (d) DAPI, Ki67, and pH3. Statistical significance was determined from multiple imaged fields from N= 3 wells and $p < 0.05$ using a one-way ANOVA and Tukey's post-hoc comparison for each cell-cycle stage separately $^{*}p < 0.05$, $^{**}p < 0.01$, $^{***}p < 0.001$, $^{****}p < 0.0001$.

NOC18 + tranilast; $p < 0.0001$; Mitosis, F (4,53) = 21.08; n = 14 control, n = 10 NOC18, n = 12 probenecid, n = 11 tranilast, n = 11 NOC18 + tranilsst; $p < 0.0001$). In contrast, treatment with the TRPV2 channel inhibitor tranilast brought about a significantly larger percentage of dividing WT microglia that expressed Ki67 and/or pH3 when compared to control WT microglia (Figures 4c and Figures 4d; one-way ANOVA; Interphase, F (4,53) = 32.28; $p < 0.0001$; Mitosis, F (4,53) = 21.08; $p < 0.0001$). Notably, WT microglia treated with both NOC18 and tranilast exhibited a significantly larger percentage of dividing microglia that expressed Ki67 and/or pH3 (Figures 4c and Figures 4d; one-way ANOVA; Interphase, F (4,53) = 32.28; $p < 0.0001$; Mitosis, F (4,53) = 21.08; $p < 0.0001$). These results demonstrate that NO inhibits microglia cell-cycle progression through TRPV2 channel activity.

Our assays further demonstrated that $iNOS^{-/-}$ microglia treated with NOC18 exhibited a significantly larger percentage of nondividing cells (Figures 5a and Figures 5b; one-way ANOVA; F (4,50) = 20.79; n = 11 control, n = 12 NOC18, n = 11 probenecid, n = 11 tranilast, n = 10 NOC18 + tranilast; $p < 0.0001$), and significantly smaller percentage of dividing microglia when compared to control (Figures 5c and Figures 5d; Interphase, F (4,50) = 15.70; n = 11 control,

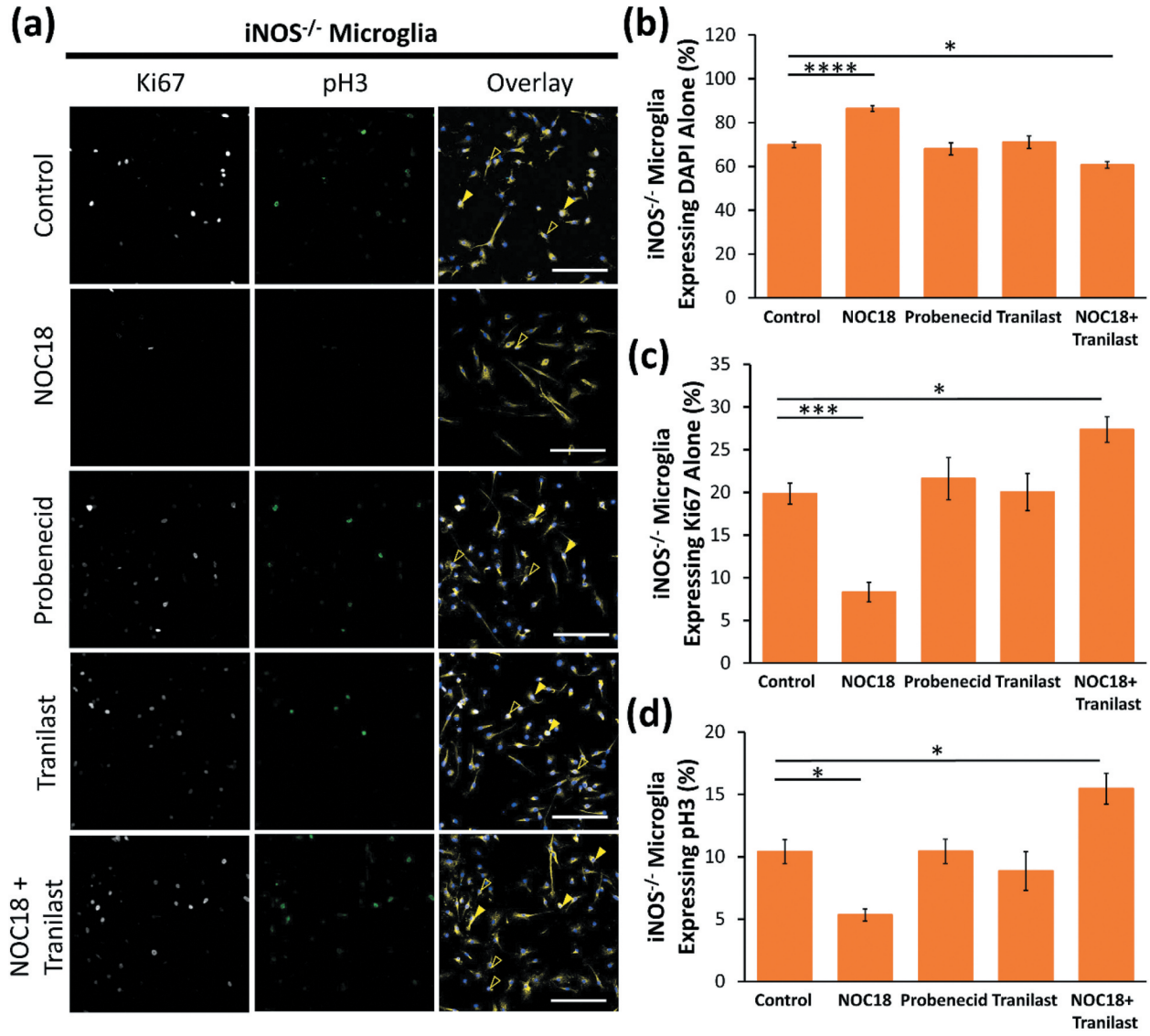

Figure 5. NO signaling influences cell-cycle progression in iNOS$^{-/-}$ microglia through TRPV2 channel activity. (a) Representative images of Ki67 (gray), pH3 (green), CD11b (yellow), and DAPI fluorescence in iNOS$^{-/-}$ microglia under control conditions or treated with NOC18 (100 µM), the TRPV2 agonist probenecid (100 µM), the TRPV2 antagonist tranilast (75 µM), or a combination of NOC18 + tranilast for 48hrs. Scale bars represent 100 µm. Open arrows point to Ki67^{+} microglia while closed arrows point to pH3^{+} microglia. Bar graphs report the percentages ± SEM of iNOS$^{-/-}$ microglia having nuclei stained with (b) DAPI alone, (c) DAPI and Ki67, or (d) DAPI, Ki67, and pH3. Statistical significance was determined from multiple imaged fields from N= 3 wells and $p < 0.05$ using a one-way ANOVA and Tukey's post-hoc comparison for each cell-cycle stage separately. *$p < 0.05$, ***$p < 0.001$, ****$p < 0.0001$.

n = 12 NOC18, n = 11 probenecid, n = 11 tranilast, n = 10 NOC18 + tranilast; $p < 0.0001$; Mitosis, F (4,50) = 11.24; n = 11 control, n = 12 NOC18, n = 11 probenecid, n = 11 tranilast, n = 10 NOC18 + tranilast; $p < 0.0001$). Activating or inhibiting TRPV2 channels with probenecid or tranilast, respectively, had no effect on the percentages of dividing or nondividing iNOS$^{-/-}$ microglia (Figure 5b– d). However, application of both NOC18 and tranilast significantly increased the percentage of actively dividing iNOS$^{-/-}$ microglia (Figures 5b and Figures 5c; Interphase, F (4,50) = 15.70; $p < 0.0001$; Mitosis, F (4,50) = 11.24; $p < 0.0001$). Taken together, this data demonstrates that iNOS/NO signaling promotes TRPV2 channel activity to restrict cell-cycle progression of microglia.

Nuclear localization and expression of NFATC2 in murine microglia are determined by TRPV2 channel activity

NFATC2 is a calcium-dependent transcription factor known to negatively regulate proliferation

[25,26]. To examine whether calcium influx through TRPV2 channels influences microglial cell-cycle progression and proliferation, we carried out immunocytochemistry to examine the subcellular localization of NFATC2 in WT and iNOS$^{-/-}$ microglia and performed immunoblot assays to analyze NFATC2 protein expression in BV2 microglia, in response to treatments with NOC18, probenecid, tranilast, or a combination of NOC18 + tranilast (Figure 6). Results from these assays demonstrated that NOC-18 treatment significantly increased the nuclear localization of NFATC2 in WT (Figures 6a and Figures 6b; one-way ANOVA, F (4,686) = 30.98; n = 165 control, n = 106 NOC18, n = 192 probenecid, n 131 tranilast, n = 97 NOC18 + tranilast; $p < 0.0001$)

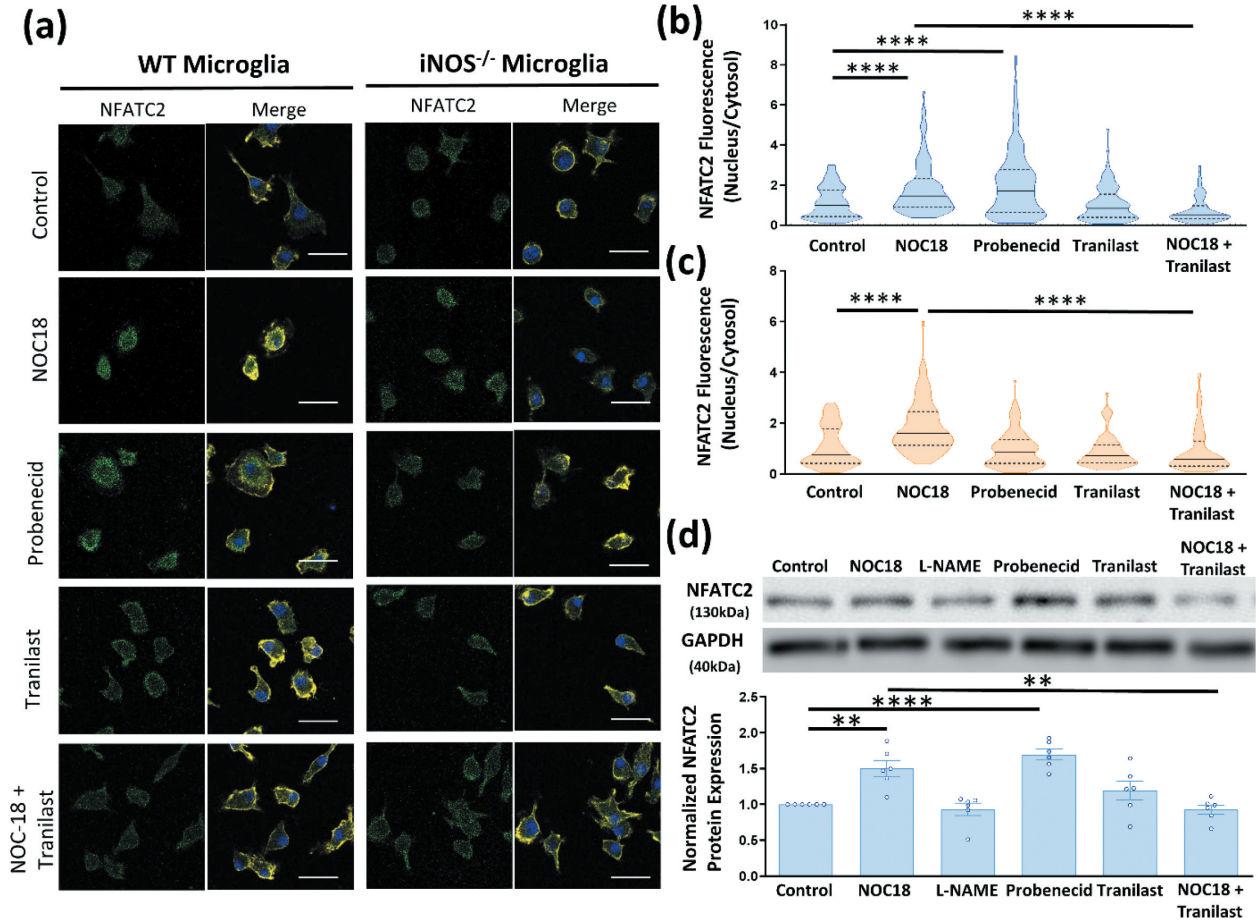

Figure 6. Nuclear localization and expression of NFATC2 in murine microglia are determined by TRPV2 channel activity. (a) Representative confocal images of NFATC2 (green), CD11b (yellow), and DAPI (blue) fluorescence in WT (Left two panels) and iNOS$^{-/-}$ (right two panels) microglia under control conditions or treatments with NOC18 (100 µM), probenecid (100 µM), tranilast (75 µM), or NOC18 + tranilast for 48hrs. Scale bars represent 50 µm. Violin plots depict the ratio of nuclear versus cytoplasmic fluorescence of NFATC2 in arbitrary units as a distribution of all (b) WT and (c) iNOS$^{-/-}$ microglia under different treatment conditions. Solid black lines indicate median values while dotted lines indicate interquartile ranges for each treatment condition. (d) *top panel*: Immunoblot of NFATC2 protein in control BV2 microglia and in response to NOC18 (100 µM), L-NAME (100 µM), probenecid (100 µM), tranilast (75 µM), or NOC18 + tranilast. GAPDH protein levels were used as a loading control. *Bottom panel*: Scatter dot plot reports the NFATC2 protein expression divided by the GAPDH protein expression and normalized to the control condition (mean ± SEM). Statistical significance for (b) and (c) was determined from n = 165 control WT cells; n = 106 NOC18 treated WT cells; n = 192 probenecid treated WT cells; n = 131 tranilast treated WT cells; n = 97 NOC18 + tranilast treated WT cells; and n = 63 control iNOS$^{-/-}$ cells; n = 96 NOC18 treated iNOS$^{-/-}$ cells; n = 146 probenecid treated iNOS$^{-/-}$ cells; n = 77 tranilast treated iNOS$^{-/-}$ cells; n = 84 NOC18 + Tranilast treated iNOS$^{-/-}$ cells from N= 4 wells while statistical significance for (d) was determined from N= 6 wells using a one-way ANOVA and Tukey's post-hoc comparison. **$p < 0.01$, ****$p < 0.0001$.

and iNOS$^{-/-}$ microglia (Figures 6a and Figures 6c; one way ANOVA, F (4,461) = 23.06; n = 63 control, n = 96 NOC18, n = 146 probenecid, n = 77 tranilast, n = 84 NOC18 + tranilast; $p < 0.0001$), and increased NFATC2 protein expression within BV2 microglia (Figure 6d; one way ANOVA, F (5,30) = 13.18; n = 6, $p < 0.0001$) when compared to controls. Treating BV2 microglia with the iNOS inhibitor L-NAME had no substantial effect on NFATC2 protein expression when compared to control (Figure 6d). The TRPV2 agonist probenecid significantly increased the nuclear localization of NFATC2 in WT microglia (Figures 6a and Figures 6b; one-way ANOVA, F (4,686) = 30.98; $p < 0.0001$) and the total protein expression of NFATC2 in BV2 microglia (Figure 6d; one-way ANOVA, F (5,30) = 13.18; n = 6; $p < 0.0001$), when compared to controls. However, probenecid had no effect on NFATC2 nuclear localization in iNOS$^{-/-}$ microglia when compared to controls (Figures 6a and Figures 6c). Blocking TRPV2 channel activity with tranilast did not affect NFATC2 nuclear localization in WT and iNOS$^{-/-}$ microglia, or protein expression in BV2 cells when compared to controls (Figure 6). However, tranilast abolished the NOC18-induced increased nuclear localization of NFATC2 in WT and iNOS$^{-/-}$ microglia (Figure 6a-c), and increased protein expression in BV2 microglia (Figure 6d). Together, these data imply that NO-facilitated TRPV2 channel activity induces the nuclear translocation and expression of NFATC2 in murine microglia.

NO-TRPV2 signaling regulates p21 transcription in WT and iNOS$^{-/-}$ murine microglia

Cell-cycle progression from G1/S and G2/M is critically controlled by the cyclin-dependent kinase inhibitor p21. Considering that the gene expression of p21 is under control by NFATC2 and that the percentage of interphase and mitotic microglia declined in response to NO or TRPV2 channel activity, we next examined whether the NO-TRPV2 dependent activation of NFATC2 regulates the mRNA expression of the cyclin-dependent kinase inhibitor p21 within primary

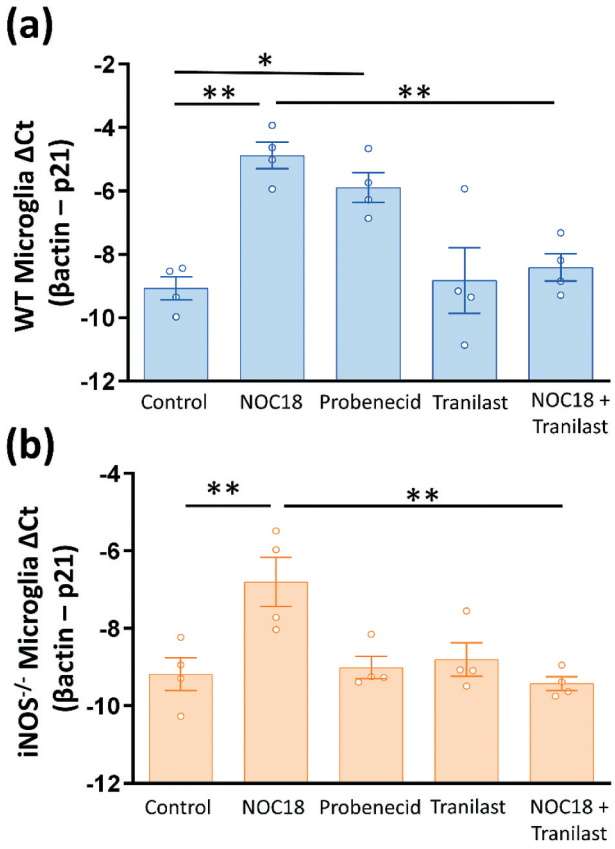

Figure 7. NO-mediated TRPV2 signaling regulates p21 transcription in primary WT and iNOS$^{-/-}$ murine microglia. Scatter dot plots report ΔCt values as mean ± SEM of p21 mRNA in relation to β-actin mRNA within primary (a) WT or (b) iNOS$^{-/-}$ microglia cultures under control conditions or treated with NOC18 (100 μM), probenecid (100 μM), tranilast (75 μM), or NOC18 + tranialst for 48 hrs. Statistical significance was determined from N= 4 wells using a one-way ANOVA and Tukey's post-hoc comparison for WT and iNOS$^{-/-}$ microglia separately *$p < 0.05$, **$p < 0.01$, ***$p < 0.001$.

microglia. Specifically, we used RT-qPCR to assay the level of p21 mRNA within WT and iNOS$^{-/-}$ microglia in response to treatment with NOC18, probenecid, tranilast, or NOC18 + tranilast (Figure 7). Results demonstrated that NOC18 treatment significantly increased the level of p21 mRNA in both WT and iNOS$^{-/-}$ microglia when compared to their respective control (Figures 7a and Figures 7b; one-way ANOVA; WT, F (4,15) = 10.6; n = 4; p = 0.0003; iNOS$^{-/-}$, F (4,15) = 6.358; n = 4; p = 0.0034). Importantly, probenecid treatment significantly increased the p21 expression in WT microglia (Figure 7a; one-way ANOVA, F (4,15) = 10.6; n = 4; p = 0.0003), but not in iNOS$^{-/-}$ microglia (Figure 7b; one-way ANOVA; F (4,15) = 6.358;

n = 4; p = 0.0034). Moreover, tranilast treatment displayed no significant effect on the levels of p21 mRNA in WT and iNOS$^{-/-}$ microglia when compared to controls (Figures 7a and Figures 7b; one-way ANOVA; WT, F (4,15) = 10.6; n = 4; p = 0.0003; iNOS$^{-/-}$, F (4,15) = 6.358; n = 4; p = 0.0034).). However, tranilast abolished the increased p21 mRNA observed from NOC18 treatment alone (Figures 7a and Figures 7b). Together, these data suggest that the NO-TRPV2-NFATC2 signaling cascade induces transcription of p21 mRNA in primary murine microglia.

Discussion

An increase of NO is well-known to restrict proliferation of many cell types including microglia [18,27–30]. We previously reported that murine microglia possess an NO-sGC-cGMP-PKG signaling cascade that arrests cell-cycle progression at the G0 stage [18]. In the present study, we are the first to demonstrate a mechanism through which iNOS/NO signaling regulates the cell-cycle progression of murine microglia. Specifically, nondividing murine microglia produced a higher level of NO, expressed more TRPV2 channel proteins on the plasma membrane, and displayed more calcium influx through TRPV2 channels than dividing microglia. Additionally, increasing NO or TRPV2 activity induced the nuclear translocation of NFATC2 and the transcription of the cyclin-dependent kinase inhibitor p21.

Microglia uptake L-arginine through the activity of the cationic amino acid transporter-1 [31,32]. The iNOS enzyme catalyzes cytosolic L-arginine into citrulline and NO [18,27–30]. In this study, we performed DAX-J2 fluorescent imaging before and after application of L-arginine to measure the production of NO in murine microglia that were at different cell-cycle stages. Our assays demonstrated that following administration of L-arginine, nondividing murine microglia produced higher levels of NO than that of dividing microglia. The production of endogenous NO depends on both the availability of L-arginine within the cell, as well as the activity of the enzymes that compete to catabolize L-arginine, including iNOS and arginase [33]. For example, L-arginine can also be catabolized by arginase into L-ornithine, a non-proteinogenic amino acid that is important for polyamine production, cell growth, and proliferation [34–36]. These distinct and opposing pathways for L-arginine metabolism may regulate microglia proliferation and cell division. We have demonstrated that iNOS activity and NO production are critically associated with microglia proliferation [18]. However, little is known about the role of arginase in the regulation of different cell-cycle stages. Given the important role of arginase in promoting cell proliferation [37,38], further studies may greatly benefit from examining the mechanisms surrounding L-arginine metabolism in cell-cycle progression.

Calcium signaling must be tightly regulated to properly progress the cell through the different stages of the cell cycle [39–41]. We previously showed that NO signals through PKG to enhance the plasma membrane expression of TRPV2 channels in murine microglia [2]. Consistent with our previous report, assays in this study demonstrated that nondividing microglia displayed a higher intensity of TRPV2 immunofluorescence on the plasma membrane, and more calcium influx through TRPV2 channels when compared to dividing microglia. On the other hand, dividing microglia had no increase in NO production after application of L-arginine, and displayed a significantly smaller calcium influx through TRPV2 channels. It is interesting to note that the amplitude of calcium influx through TRPV2 channels in WT microglia was sustained after nine minutes in all cell-cycle stages, while the calcium influx through TRPV2 channels in iNOS$^{-/-}$ microglia was transient and began to decline after 9 min in all cell-cycle stages. In regard to this phenomenon, it was reported that TRPV2 channels are gated by phosphatidylinositol 4,5, bisphosphate (PIP_2), a membrane phospholipid [42], and that catabolism of PIP_2 is reduced in the presence of NO [43]. Therefore, the more abundant PIP_2 in WT microglia may gate and contribute to the sustained calcium influx through TRPV2 channels that were observed in WT microglia and not in iNOS$^{-/-}$ microglia.

The presence of TRPV2 activity in iNOS$^{-/-}$ microglia may be attributed to the addition of fetal bovine growth serum in the culture media, as growth factors increase the plasma membrane expression of TRPV proteins [44–46]. Additionally, NO can regulate mitogenic growth factor receptors and their downstream pathways to influence cell proliferation [47,48]. Therefore, the different calcium influx kinetics observed through TRPV2 channels between WT and iNOS$^{-/-}$ microglia may stem from the regulation of mitogenic growth factor receptors and/or PIP_2 gating of TRPV2 channels by NO signaling.

It has been reported that TRPV2 channel activity critically regulates cell proliferation, differentiation, and cancer progression [19–22,39]. For example, decreased TRPV2 expression and/or activity enhances astrocyte proliferation and contributes to glioma growth [20,21,39]. Consistent with these results, our assays demonstrated that stimulating TRPV2 channels in WT microglia decreased the percentage of dividing microglia, whereas inhibiting TRPV2 channels increased the percentage of dividing microglia when compared to controls. On the other hand, activating or inhibiting TRPV2 channels in iNOS$^{-/-}$ microglia had no significant effect

on the percentage of microglia dividing. The diminished response to the TRPV2 channel modulators on iNOS$^{-/-}$ microglia cell-cycle progression is substantiated by the reduced plasma membrane expression of TRPV2 channels observed in iNOS$^{-/-}$ microglia.

We have reported that NO facilitates TRPV2 translocation to the plasma membrane in murine microglia [2]. Considering that nondividing microglia displayed larger NO production and elevated calcium influx through TRPV2 channels when compared to dividing microglia, we examined whether NO restricts cell-cycle progression by enhancing TRPV2 activity in microglia. Our assays showed that application of the NO-donor NOC18 or the TRPV2 channel agonist probenecid significantly decreased the percentage of dividing WT microglia, while application of the TRPV2 channel antagonist tranilast increased the percentage of dividing WT microglia in culture. Moreover, blocking TRPV2 channels in WT microglia not only abolished the NOC18-induced increase in nondividing cells, but also significantly increased the percentage of dividing WT microglia in culture. All these results demonstrate that NO restricts microglia proliferation by enhancing TRPV2 channel activity.

Although application of 2APB evoked a transient calcium influx through TRPV2 channels in iNOS$^{-/-}$ microglia, treatment with a selective TRPV2 agonist or antagonist had no effect on the cell-cycle progression of iNOS$^{-/-}$ microglia. These results indicate that the lack of endogenous NO signaling in murine microglia leads to inadequate TRPV2 channel activity that does not alter cell-cycle progression. It is important to note that application of the NO-donor NOC18 still significantly increased the percentage of nondividing iNOS$^{-/-}$ microglia in culture. However, blocking TRPV2 channels in iNOS$^{-/-}$ microglia not only abolished the NOC18-induced increase in nondividing cells, but unexpectedly increased the percentage of dividing iNOS$^{-/-}$ microglia when compared to controls. These results demonstrate a complex role of endogenous iNOS/NO signaling in microglia proliferation that requires further studies. For example, it is reported that NO-induced nitrosylation of Cys^{118} of p21RAS, a protein that promotes cell-cycle progression and cell proliferation, enhanced the proliferation of human breast cancer cells [49,50]. Therefore, in addition to activating the PKG-TRPV2 signaling cascade to inhibit proliferation in microglia, exogenous NO may also enhance the cell-cycle progression of microglia through an alternative secondary mechanism that is independent of PKG-TRPV2 signaling, like we previously observed [18].

It is reported that TRPV2 channel activity negatively regulates proliferation and enhances cell differentiation through the activation of NFAT transcription factors [51–54]. Specifically, calcium influx through TRPV2 channels induces calmodulin-dependent activation of calcineurin and dephosphorylation, activation, and nuclear translocation of NFATs in osteoclast differentiation [51]. Along those lines, activation of TRPV2 channels increases differentiation of brown adipose tissue [55], and inhibits proliferation of astrocytes and gliomas [20–22]. Importantly, the most abundant NFAT isoform in microglia is NFATC2 [56]. NFATC2 promotes differentiation [54] and cell-cycle arrest by decreasing the expression of cyclin-dependent kinase-4 [57] and cyclin-A2 [26,52], and by increasing the expression of the cyclin-dependent kinase inhibitor p21 [53,58]. Therefore, we examined NFATC2 subcellular localization and p21 mRNA expression to understand the mechanism by which NO-TRPV2 signaling restricts microglia cell-cycle progression.

In the present study, we observed that NOC18 treatment on primary microglia and BV2 cells significantly increased NFATC2 nuclear localization and protein expression when compared to controls, respectively. Additionally, agonizing TRPV2 channels on WT and BV2 microglia increased NFATC2 nuclear localization and protein expression when compared to controls, respectively. In contrast, agonizing TRPV2 channels on iNOS$^{-/-}$ microglia did not significantly influence NFATC2 nuclear translocation, likely due to the decreased TRPV2 plasma membrane expression observed in iNOS$^{-/-}$ microglia. Furthermore, antagonizing TRPV2 channels in the presence of NOC18 had no effect on NFATC2 nuclear localization, or protein expression in BV2 microglia. Furthermore, our assays demonstrated that NFATC2 nuclear translocation in murine microglia was associated with increased transcriptional levels of p21, a potent cyclin-dependent kinase inhibitor that arrests cell-cycle progression in G0 [58].

In summary, we have demonstrated for the first time that nondividing microglia in G0 displayed higher levels of NO production, plasma membrane expression of TRPV2, calcium influx through TRPV2 channels, NFATC2 nuclear localization, and transcription of p21. As illustrated in Figure 8, we proposed a molecular mechanism by which NO restricts the cell-cycle progression of murine microglia. Briefly, microglia in G0 produce an elevated level of NO that signals through the classical PKG signaling cascade to promote TRPV2 translocation to the plasma membrane [2]. The increased calcium influx through TRPV2 channels activates the calmodulin-dependent phosphatase calcineurin that dephosphorylates and activates NFATC2 [53]. Activated NFATC2 translocates into the nucleus to initiate the transcription of the cyclin-dependent kinase inhibitor p21 [58], which results in cell-cycle arrest [58]. In contrast, reduced iNOS/NO signaling enhances microglia proliferation and this excessive microglia proliferation may contribute to the pathological progressions of certain neurological diseases such as glioma [5,11–13].

Acknowledgments

This work was supported by the Canadian Institutes of Health Research (MOP-133504) awarded to W-Y L. MJEM and VT have been awarded Ontario Graduate Scholarships.

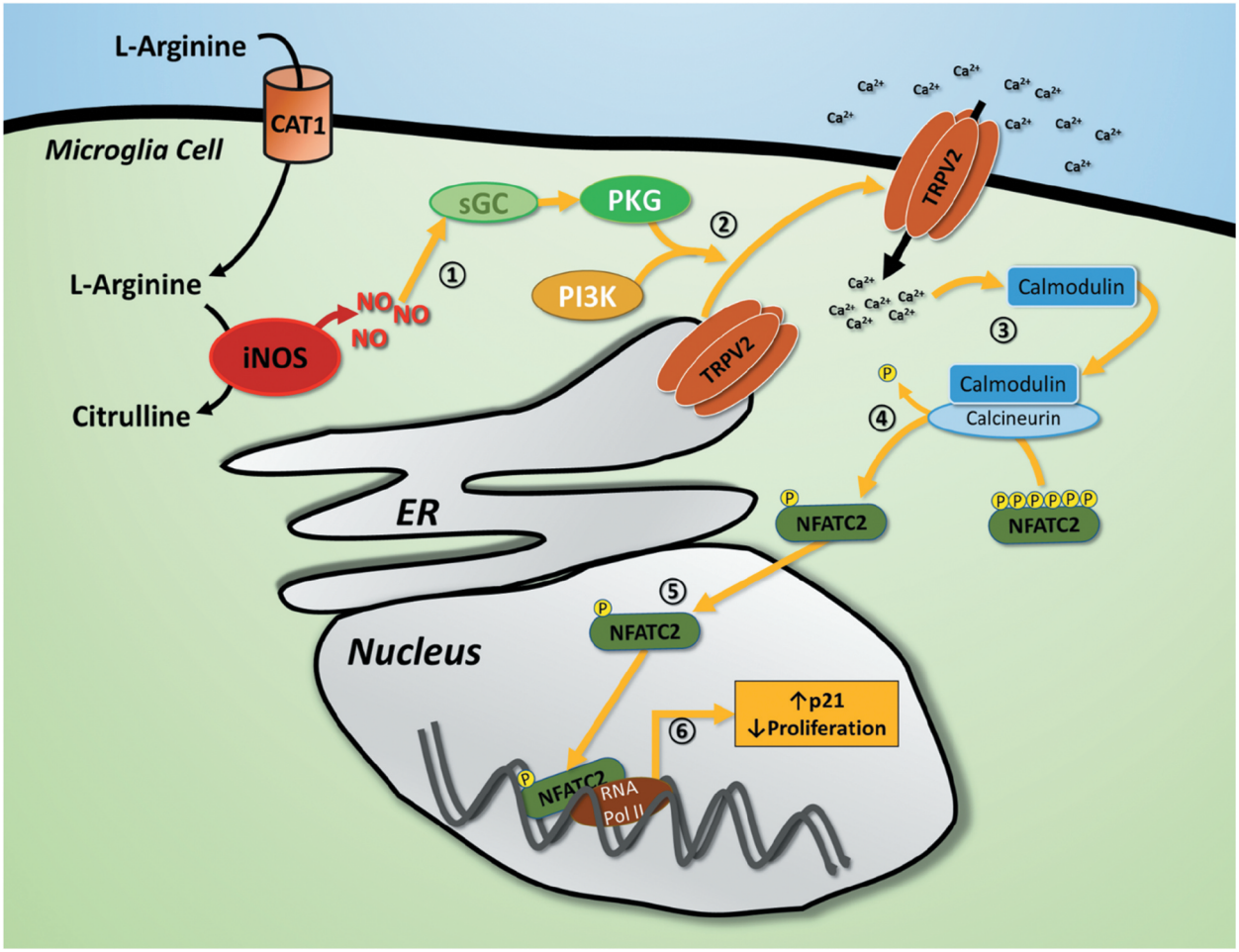

Figure 8. Proposed molecular mechanism by which NO-signaling restricts microglial cell-cycle progression. (1) Microglia produce L-arginine as a product of the urea cycle or take up exogenous L-arginine through the activity of the cationic amino acid transporter-1 (CAT1). iNOS activity in microglia catabolizes the substrate L-arginine into citrulline and NO. NO binds and activates sGC to produce cGMP, which binds and activates PKG. **(2)** PKG activity in combination with PI3K induce the trafficking of TRPV2 ion channels from the ER/Golgi to the plasma membrane as previously described [2]. **(3)** Calcium influx through TRPV2 channels promote calcium-calmodulin binding to the phosphatase calcineurin. **(4)** Activated calcineurin dephosphorylates NFATC2. **(5)** Activated NFATC2 translocates from the cytoplasm to the nucleus. **(6)** NFATC2 in the nucleus promotes transcription of the cyclin dependent kinase inhibitor p21 and inhibits microglial proliferation.

Disclosure statement

The authors report no conflict of interest.

Funding

This work was supported by the Canadian Institutes of Health Research [MOP-133504].

Data availability statement

The data that support the findings of this study are available from the corresponding author, WYL, upon reasonable request.

References

[1] Biber K, Owens T, Boddeke E. What is microglia neurotoxicity (Not)? Glia. 2014;62:841–854.
[2] Maksoud MJE, Tellios V, An D, et al. Nitric oxide upregulates microglia phagocytosis and increases transient receptor potential vanilloid type 2 channel expression on the plasma membrane. Glia. 2019;67:2294–2311.
[3] Saha RN, Pahan K. Regulation of inducible nitric oxide synthase gene in glial cells. Antioxid Redox Signal. 2006;8:929–947.
[4] Traister A, Abashidze S, Gold V, et al. Evidence that nitric oxide regulates cell-cycle progression in the developing chick neuroepithelium. Dev Dyn. 2002;225:271–276.

[5] Simmons GW, Pong WW, Emnett RJ, et al. Neurofibromatosis-1 heterozygosity increases microglia in a spatially and temporally restricted pattern relevant to mouse optic glioma formation and growth. J Neuropathol Exp Neurol. 2011;70:51–62.
[6] He BP, Wang JJ, Zhang X, et al. Differential reactions of microglia to brain metastasis of lung cancer. Mol Med. 2006;12:161–170.
[7] Kim YJ, Hwang SY, Han IO. Insoluble matrix components of glioma cells suppress LPS-mediated iNOS/NO induction in microglia. Biochem Biophys Res Commun. 2006;347:731–738.
[8] Komohara Y, Ohnishi K, Kuratsu J, et al. Possible involvement of the M2 anti-inflammatory macrophage phenotype in growth of human gliomas. J Pathol. 2008;216:15–24.
[9] Qiu B, Zhang D, Wang C, et al. IL-10 and TGF-β2 are overexpressed in tumor spheres cultured from human gliomas. Mol Biol Rep. 2011;38:3585–3591.
[10] Zhang L, Handel M, Schartner J, et al. Regulation of IL-10 expression by upstream stimulating factor (USF-1) in glioma-associated microglia. J Neuroimmunol. 2007;184:188–197.
[11] Badie B, Schartner JM. Flow cytometric characterization of tumor-associated macrophages in experimental gliomas. Neurosurgery. 2000;46:957–962.
[12] Morimura T, Neuchrist C, Kitz K, et al. Monocyte subpopulations in human gliomas: expression of Fc and complement receptors and correlation with tumor proliferation. Acta Neuropathol. 1990;80:287–294.
[13] Roggendorf W, Strupp S, Paulus W. Distribution and characterization of microglia/macrophages in human brain tumors. Acta Neuropathol. 1996;92:288–293.
[14] Kamphuis W, Orre M, Kooijman L, et al. Differential cell proliferation in the cortex of the appsweps1de9 alzheimer's disease mouse model. Glia. 2012;60:615–629.
[15] Togo T, Katsuse O, Iseki E. Nitric oxide pathways in Alzheimer's disease and other neurodegenerative dementias. Neurol Res. 2004;26:563–566.
[16] Wilcock DM, Lewis MR, Van Nostrand WE, et al. Progression of amyloid pathology to Alzheimer's disease pathology in an amyloid precursor protein transgenic mouse model by removal of nitric oxide synthase 2. J Neurosci. 2008;28:1537–1545.
[17] Engler JR, Robinson AE, Smirnov I, et al. Increased microglia/macrophage gene expression in a subset of adult and pediatric astrocytomas Jones C, ed. PLoS One. 2012;7:e43339.
[18] Maksoud MJE, Tellios V, Xiang -Y-Y, et al., Nitric oxide signaling inhibits microglia proliferation by activation of protein kinase-G. Nitric Oxide 2020;94:125–134.
[19] Liberati S, Morelli M, Amantini C, et al. Loss of TRPV2 homeostatic control of cell proliferation drives tumor progression. Cells. 2014;3:112–128.
[20] Morelli MB, Nabissi M, Amantini C, et al. The transient receptor potential vanilloid-2 cation channel impairs glioblastoma stem-like cell proliferation and promotes differentiation. Int J Cancer. 2012;131:E1067–E1077.
[21] Nabissi M, Morelli MB, Amantini C, et al. TRPV2 channel negatively controls glioma cell proliferation and resistance to Fas-induced apoptosis in ERK-dependent manner. Carcinogenesis. 2010;31:794–803.
[22] Zhang H, Xiao J, Hu Z, et al. Blocking transient receptor potential vanilloid 2 channel in astrocytes enhances astrocyte-mediated neuroprotection after oxygen–glucose deprivation and reoxygenation. Eur J Neurosci. 2016;44:2493–2503.
[23] Schindelin J, Arganda-Carreras I, Frise E, et al. Fiji: an open-source platform for biological-image analysis. Nat Methods. 2012;9:676–682.
[24] Cao T, Ramsey IS. Toll-Like receptor 4 activation by LPS stimulates TRPV2 channel activity in microglia. Biophys J. 2016;110:286a.
[25] Baksh S, DeCaprio JA, Burakoff SJ. Calcineurin regulation of the mammalian G0/G1 checkpoint element, cyclin dependent kinase 4. Oncogene. 2000;19:2820–2827.
[26] Carvalho LDS, Teixeira LK, Carrossini N, et al. The NFAT1 transcription factor is a repressor of cyclin A2 gene expression. Cell Cycle. 2007;6:1789–1795.
[27] Garg CU, Hassid A. Rapid publication nitric oxide-generating vasodilators and 8-Bromo-Cyclic guanosine monophosphate inhibit mitogenesis and proliferation of cultured rat vascular smooth muscle cells. J Clin Invest. 1989;84:1774–1777.
[28] Kawahara K, Gotoh T, Oyadomari S, et al. Nitric oxide inhibits the proliferation of murine microglial MG5 cells by a mechanism involving p21 but independent of p53 and cyclic guanosine monophosphate. Neurosci Lett. 2001b;310:89–92.
[29] MacMicking J, Xie QW, Nathan C. Nitric oxide and macrophage function. Annu Rev Immunol. 1997;15:323–350.
[30] Tate DJ, Patterson JR, Velasco-Gonzalez C, et al. Interferon-gamma-induced nitric oxide inhibits the proliferation of murine renal cell carcinoma cells. Int J Biol Sci. 2012;8::1109–1120.
[31] Czapiga M, Colton C. Microglial function in human APOE3 and APOE4 transgenic mice: altered arginine transport. J Neuroimmunol. 2003;134:44–51.
[32] Kawahara K, Gotoh T, Oyadomari S, et al. Co-induction of argininosuccinate synthetase, cationic amino acid transporter-2, and nitric oxide synthase in activated murine microglial cells. Mol Brain Res. 2001a;90:165–173.

[33] Pautz A, Art J, Hahn S, et al. Regulation of the expression of inducible nitric oxide synthase. Nitric Oxide - Biol Chem. 2010;23:75–93.
[34] Li H, Meininger CJ, Bazer FW, et al. Intracellular sources of ornithine for polyamine synthesis in endothelial cells. Amino Acids. 2016;48:2401–2410.
[35] Medina-Enríquez MM, Alcántara-Farfán V, Aguilar-Faisal L, et al. N-ω-chloroacetyl-l-ornithine, a new competitive inhibitor of ornithine decarboxylase, induces selective growth inhibition and cytotoxicity on human cancer cells versus normal cells. J Enzyme Inhib Med Chem. 2015;30:345–353.
[36] Soda K. The mechanisms by which polyamines accelerate tumor spread. J Exp Clin Cancer Res. 2011;30:95.
[37] Chang CI, Liao JC, Kuo L. Macrophage arginase promotes tumor cell growth and suppresses nitric oxide-mediated tumor cytotoxicity. Cancer Res. 2001;61:1100–1106.
[38] Wei LH, Wu G, Morris SM, et al. Elevated arginase I expression in rat aortic smooth muscle cells increases cell proliferation. Proc Natl Acad Sci. 2001;98:9260–9264.
[39] Cui C, Merritt R, Fu L, et al. Targeting calcium signaling in cancer therapy. Acta Pharm Sin B. 2017;7:3–17.
[40] Koledova VV, Khalil RA. Ca2+, calmodulin, and cyclins in vascular smooth muscle cell cycle. Circ Res. 2006;98:1240–1243.
[41] Lu KP, Means AR. Regulation of the cell cycle by calcium and calmodulin. Endocr Rev. 1993;14:40–58.
[42] Mercado J, Gordon-Shaag A, Zagotta WN, et al. Ca2+-Dependent Desensitization of TRPV2 Channels Is Mediated by Hydrolysis of Phosphatidylinositol 4,5-Bisphosphate. J Neurosci. 2010;30:13338–13347.
[43] Clementi E, Sciorati C, Riccio M, et al. Nitric Oxide Action on Growth Factor-elicited Signals. J Biol Chem. 1995;270:22277–22282.
[44] Nagasawa M, Kojima I. Translocation of calcium-permeable TRPV2 channel to the podosome: its role in the regulation of podosome assembly. Cell Calcium. 2012;51:186–193.
[45] Nagasawa M, Nakagawa Y, Tanaka S, et al. Chemotactic peptide fMetLeuPhe induces translocation of the TRPV2 channel in macrophages. J Cell Physiol. 2007;210:692–702.
[46] Perálvarez-Marín A, Doñate-Macian P, Gaudet R. What do we know about the transient receptor potential vanilloid 2 (TRPV2) ion channel? Febs J. 2013;280:5471–5487.
[47] Parenti A, Morbidelli L, Cui X-L, et al. Nitric oxide is an upstream signal of vascular endothelial growth factor-induced extracellular signal-regulated Kinase½ activation in postcapillary endothelium. J Biol Chem. 1998;273:4220–4226.
[48] Villalobo A. Review article: nitric oxide and cell proliferation. Febs J. 2006;273:2329–2344.
[49] Heo J, Prutzman KC, Mocanu V, et al. Mechanism of free radical nitric oxide-mediated ras guanine nucleotide dissociation. J Mol Biol. 2005;346:1423–1440.
[50] Pervin S, Singh R, Hernandez E, et al. Nitric Oxide in Physiologic Concentrations Targets the Translational Machinery to Increase the Proliferation of Human Breast Cancer Cells : involvement of Mammalian Target of Rapamycin/eIF4E Pathway. Cancer Res. 2007; 289–300.
[51] Bai H, Zhu H, Yan Q, et al. TRPV2-induced Ca2+--calcineurin-NFAT signaling regulates differentiation of osteoclast in multiple myeloma. Cell Commun Signal. 2018;16:1–11.
[52] Caetano MS, Vieira-de-abreu A, Teixeira LK, et al. (2002) Control lymphocyte proliferation and cyclin A2 gene transcription by a mechanism involving the transcription factor NFAT1.
[53] Mognol GP, Carneiro FRG, Robbs BK, et al. Cell cycle and apoptosis regulation by NFAT transcription factors: new roles for an old player. Cell Death Dis. 2016;7:e2199–e2199.
[54] Robbs BK, Cruz ALS, Werneck MBF, et al. Dual roles for NFAT transcription factor genes as oncogenes and tumor suppressors. Mol Cell Biol. 2008;28:7168–7181.
[55] Sun W, Uchida K, Takahashi N, et al. Activation of TRPV2 negatively regulates the differentiation of mouse brown adipocytes. Pflügers Arch - Eur J Physiol. 2016;468:1527–1540.
[56] Manocha GD, Ghatak A, Puig KL, et al. NFATc2 modulates microglial activation in the AβPP/PS1 mouse model of Alzheimer's disease Bhat N, ed. J Alzheimer's Dis. 2017;58:775–787.
[57] Baksh S, Widlund HR, Frazer-Abel AA, et al. NFATc2-mediated repression of cyclin-dependent kinase 4 expression. Mol Cell. 2002;10:1071–1081.
[58] Santini MP, Talora C, Seki T, et al. Cross talk among calcineurin, Sp1/Sp3, and NFAT in control of p21WAF1/CIP1 expression in keratinocyte differentiation. Proc Natl Acad Sci. 2001;98:9575–9580.